https://doi.org/10.5194/egusphere-2025-31
Preprint. Discussion started: 27 January 2025

Influence of Snow Spatial Variability on Cosmic Ray Neutron SWE

Haejo Kim[1], Eric Sproles[2,3], Samuel E. Tuttle[1]

[1]Department of Earth & Environmental Sciences, Syracuse University, Syracuse, NY, 13244, USA
[2] Department of Earth Sciences, Montana State University, Bozeman, MT, 59717, USA
[3] Geospatial Core Facility, Montana State University

Correspondence to: Haejo Kim (hkim139@syr.edu)

Abstract. Monitoring prairie snow has been difficult due to its extreme spatial variability from windy conditions, gentle topography, and low tree cover. Previous work has shown that a noninvasive (or aboveground) Cosmic Ray Neutron Sensor (CRNS) placed at the Central Agricultural Research Center (CARC; 47.07º N, 109.95º W), an agricultural research site within a semi-arid prairie environment managed by Montana State University, was sensitive to both the low snow amounts and spatial variability of prairie snow. In this study, we build upon previous work to understand how different snow distributions would have influenced CRNS measurements at the CARC. Specifically, we compared the changes in neutron counts and snow water equivalent (SWE) after relocating our CRNS probe at the CARC using the Ultra Rapid Neutron-Only Simulation (URANOS) and comparing them to uniform snow distributions. For shallow, heterogeneous snowpacks like the ones observed at the CARC, the magnitude and distance of the snow drifts from the CRNS has the greatest effect on neutron counts. Therefore, the best place to site a CRNS is within areas of low snow accumulation that are nearby areas of high snow accumulation to obtain a reasonable spatial estimate. Despite this, a naive CRNS placement was 2 to 5 times more likely to yield better SWE estimates compared to snow scales or currently available gridded products. CRNS provides valuable information about shallow, heterogeneous snowpacks in prairie and other environments and can benefit future missions from UAV and satellite platforms.

1 Introduction

Seasonal snow plays an important hydrologic and climatic role in the Earth system. Seasonal snow covers an average of 31% of the Earth's surface annually (Tsang et al., 2022). A major component of the Western United States' water supply originates from seasonal snowpack, feeding the needs of over 60 million people (Bales et al., 2006). Prairie snow can make up to 25% of the global snow cover (Sturm and Liston, 2021). Mid-latitude semi-arid prairie environments, such as those found in the interior Great Plains of North America (i.e. northern states such as Montana and extending north into Canada) are dependent on snow. Over 80 to 85% of streamflow in the Northern Great Plains originates from snow (Gray, 1970), despite accounting for 20% of the annual precipitation (Aase and Siddoway, 1980).

https://doi.org/10.5194/egusphere-2025-31
Preprint. Discussion started: 27 January 2025

Snow cover in the prairie is known for its extreme spatial heterogeneity, mainly due to strong surface winds, gentle topography, and spatial variability in vegetation (Gray, 1970). Figure 1 depicts the variability that snow can exhibit in a prairie environment. Strong winds in an open, flat expanse of land scours snow, causing wind erosion, enhancing sublimation, and transporting 75% of the annual snowfall (Gray, 1970; Harder et al., 2019). The effects of blowing snow are affected by changes in surface roughness such as vegetation which allows for preferential deposition and accumulation of snow along natural barriers (Harder et al., 2019; Kort et al., 2012). These areas of preferential deposition can build snow drifts as shown in Fig. 1a that can grow over 1 m tall and can transition to bare ground over a spatial scale of meters to tens of meters.

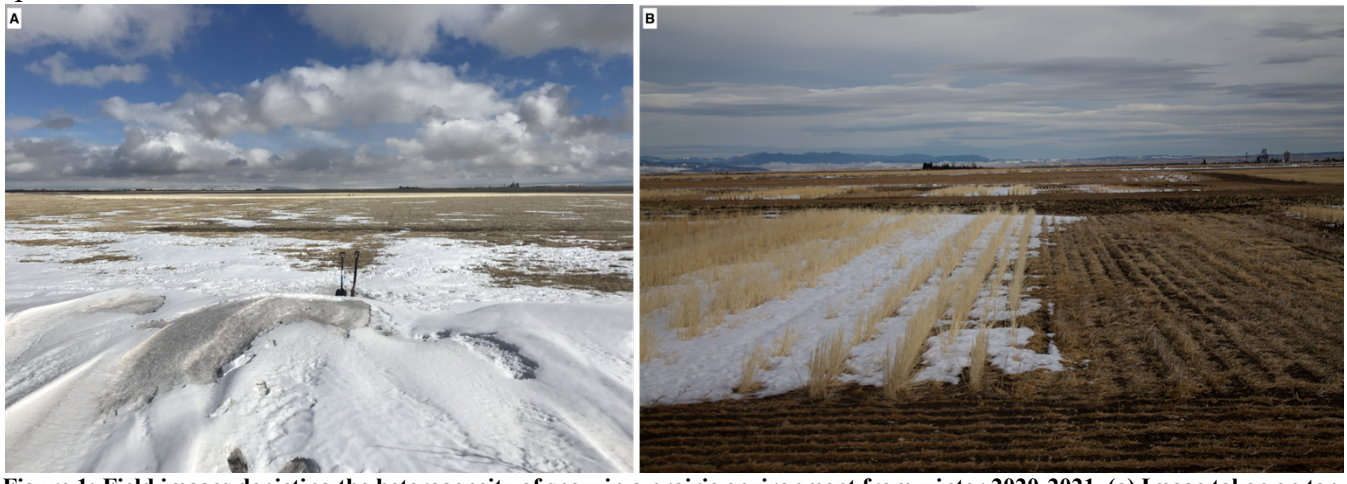

Figure 1: Field images depicting the heterogeneity of snow in a prairie environment from winter 2020-2021. (a) Image taken on top of > 1 m snow drift, looking east, with snow disappearing as you move away from the snow drift. (b) Standing crop stubble is used to trap snow for early spring melt. Field images were provided by Dr. Eric Sproles.

Agriculture and crop stubble are the most common form of land use change in the Northern Great Plains that drive preferential snow accumulation. The introduction of dryland cropping techniques, especially no till (or zero tilling) techniques where seeds are directly planted into crop residues and no tillage of soils, allows certain winter wheat crops to grow in the Northern Great Plains (Nielsen et al., 2005; Aase and Siddoway, 1980; Harder et al., 2019). Due to the semi-arid climate in the Northern Great Plains, water use must be efficient for agricultural fields to be productive. This agricultural development in the prairies has increased the need to capture snow for early season melt water. As a result, farmers use standing crop stubbles to aid in trapping snow and reducing snow erosion in order to provide water recharge and managing infiltration and runoff (see Fig. 1b) (Aase and Siddoway, 1980; Harder et al., 2019).

Snow heterogeneity introduces an important question in water resources management: How and where can we effectively measure snow water equivalent (SWE) in such an environment? Traditional manual snow measurements from snow pits are labour-intensive and are best applied in deep snow. Snow pit measurements of snow density are restricted to the snow drifts and not of the typically shallower prairie snowpack. In addition, continuous SWE monitoring through snow pillows or snow scales like those found in the snow telemetry (SNOTEL) network from the US Department of Agriculture Natural Resources Conservation Service (USDA NRCS) (Serreze et al., 1999), are not as

https://doi.org/10.5194/egusphere-2025-31
Preprint. Discussion started: 27 January 2025

effective in the prairie due to wind erosion. Additionally, Figure 1 shows how the placement of a snow pillow or snow scale (e.g. in an area that accumulates a snow drift or an area that is wind-scoured) could result in very different snow measurements, some (or all) of which may not reflect the areal average SWE.

To address these issues, we installed a Cosmic Ray Neutron Sensor (CRNS) to measure the SWE at an agricultural research site in the plains of central Montana. CRNS instruments detect the background neutron flux that is generated when cosmic rays interact with matter on Earth (Desilets et al., 2010). Hydrogen atoms are roughly the same size as neutrons, and trap the free neutrons, attenuating the signal (Zreda et al., 2012). Thus, the neutron flux measured by a detector is inversely related to the amount of hydrogen atoms in its immediate surroundings. The most common source of hydrogen in the environment are water molecules in the atmosphere (Rosolem et al., 2013; Zreda et al., 2012), vegetation (Baroni et al., 2018; Franz et al., 2015), and soils (e.g., lattice water and organic matter) (Bogena et al., 2013; Franz et al., 2013). After accounting for all other hydrogen pools, estimates of soil moisture and SWE are made over an approximate operational radius of 150 to 250 m (for aboveground CRNS) by detecting the neutron flux over time (Zreda et al., 2008; Royer et al., 2021). The non-invasive and large footprint of CRNS has intriguing potential to overcome the issues of traditional continuous snow monitoring in heterogeneous shallow to moderate snowpacks. It also helps to mitigate a common issue in hydrology: bridging the scale gap between point measurements and areal measurements, such as remote sensing or modelling studies, by providing measurements of areal SWE at an intermediate or similar spatial resolution (Blöschl, 1999; Iwema et al., 2015; Schattan et al., 2020).

Previous research has shown that CRNS estimates of SWE at an agricultural prairie site in central Montana agree with spatially weighted digital snow models (DSMs) from UAV light detection and ranging (lidar) flights and modelled CRNS estimates, despite extreme spatial heterogeneity of the snowpack surrounding the detector (Woodley et al., 2024). CRNS has been noted to be sensitive to bare ground patches, usually increasing the neutron counts (Schattan et al., 2019). We build on our previous research from Woodley et al. (2024) to analyse the effects of snow heterogeneity within the operational footprint of the CRNS using neutron transport modelling. From these results, we provide insights and guidelines on best practices to site future CRNS probes with respect to shallow, heterogenous snowpacks. Furthermore, we hope to show that CRNS measurements can be a reliable ground truth for remote sensing applications in the prairies.

2 Study Area

The modelling domain for this study is a 1 km^2 region of the Central Agricultural Research Center (CARC), an agricultural research site managed by Montana State University, located in central Montana (47.057510˚ N, 109.952945˚ W; see Fig. 2). The CARC hosts ongoing agricultural research where researchers investigate different crop varieties, cropping strategies, and soil biogeochemistry. Crops typically grown at the CARC include cereals, grasses, legumes, and broadleaf plants. Some crops persist into the winter as stubble at the CARC, depending on harvest practices (Palomaki and Sproles, 2023). The elevation of the study region ranges from 1287 m to 1298 m. Soils at the CARC are

https://doi.org/10.5194/egusphere-2025-31
Preprint. Discussion started: 27 January 2025

primarily well-drained, shallow clay loams (Palomaki and Sproles, 2023). We observed average air temperatures of -0.4°C (-3.7°C during DJF), average air pressure of 870 mb, and average relative humidity of 62.8% throughout the winter of 2020-2021. A CRNS (CRS2000/B from HydroInnova LLC, Albuquerque, NM, USA) was deployed at the site in the winter of 2020/2021, coincident with the SnowEx 2021 Prairie field campaign, to measure the low-energy cosmic ray-induced neutrons (Woodley et al., 2024).

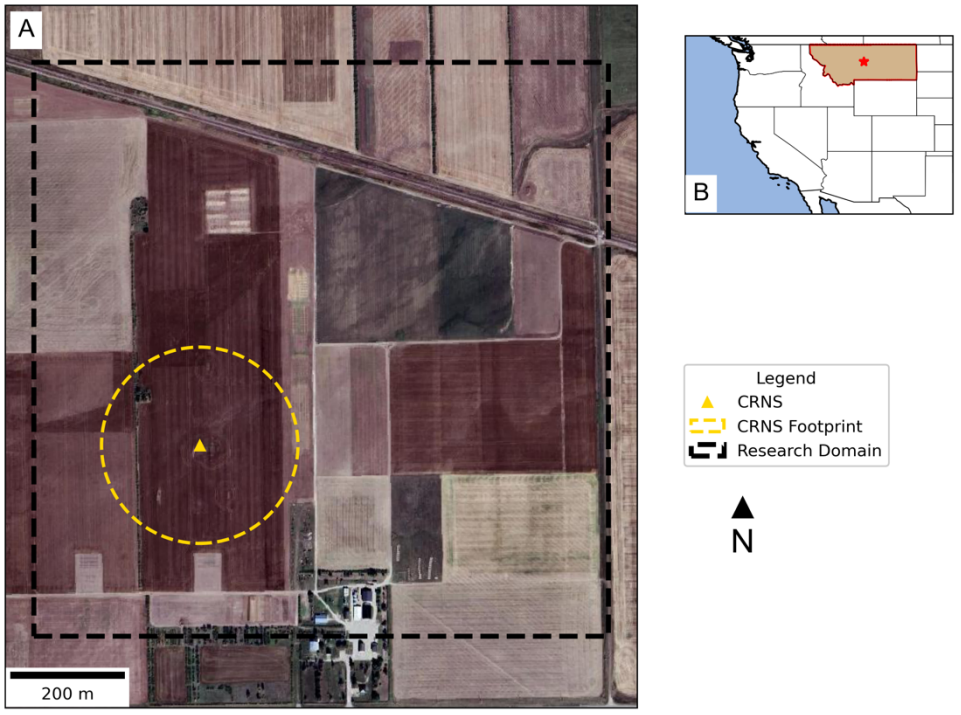

Figure 2: Basemap of study site. a) The 1 km² research domain outlined by the dashed black box at the Central Research Agricultural Center (CARC). The CRNS location is marked by the yellow triangle and the estimated 171 m footprint (calculated in Woodley et al. (2024) is shown in the dashed yellow circle. b) The approximate location of the CARC in Moccasin, MT in Central Montana is marked by the red star. The State of Montana is also highlighted in red with a fill colour of tan. (Basemap Image: © Google Maps).

3 Data and Methods

3.1 In Situ Measurements

The CARC was selected for NASA's SnowEx field campaign to study prairie snow as one of its main objectives in the winter of 2020/2021. SnowEx efforts at the CARC included airborne L-band interferometric synthetic aperture radar (InSAR) flights from the Uninhabited Aerial Vehicle Synthetic Aperture Radar (UAVSAR) instrument, snow-on and snow-off UAV lidar observations, UAV orthophotos and structure from motion (SfM), and ground-based snow observations including snow pits and snow depth transects (Palomaki and Sproles, 2023). For this analysis, we imported spatially distributed SWE into our neutron transport simulation, which was estimated using spatial distributed

https://doi.org/10.5194/egusphere-2025-31
Preprint. Discussion started: 27 January 2025

snow depth maps from the UAV lidar flights and snow density data calculated from snow pits (Woodley et al., 2024).

Table 1 summarizes the snow depths from the 8 UAV lidar flights made in winter 2020/2021 across 8 different dates in our 1 km^2 study area. The lidar measurements show how snow depths can vary spatially and temporally within the CARC. The lidar flight conducted on 15 January 2021 is considered our "no snow" baseline. Despite the large changes in snow depths due to the snow drifts, the snow drifts typically covered less than 1% of the 1 km^2 area before February 2021. The digital snow model from the UAV lidar was divided into 2 m by 2 m pixels, for a total model domain of 500 pixels by 500 pixels.

Table 1: Snow depths (SD) and the snow covered area (SCA) statistics from the digital snow models from each of the 8 UAV lidar flights at the CARC. We report the average and maximum SD for each date. The SCA is reported as the percentage of the CARC within the 1 km^2 research area is covered by snow and the percentage of the CARC covered by greater than 20 cm of snow.

Date	Avg. SD, Excluding Bare Ground (Avg. With Bare Ground) [cm]	Max. SD [cm]	SCA [%]	SCA, SD > 20 cm [%]
15 Jan. 2021	5.3 (0.1)	63.4	1.80%	0.2%
21 Jan. 2021	3.6 (1.6)	96.7	45.1%	0.6%
22 Jan. 2021	3.8 (2.0)	82.7	52.1%	0.5%
29 Jan. 2021	3.2 (0.9)	82.8	28.1%	0.5%
17 Feb. 2021	8.8 (7.9)	131.5	89.6%	5%
18 Feb. 2021	8.7 (7.6)	131	87.1%	4.8%
24 Feb. 2021	5.5 (2.2)	100.6	39.7%	2.4%
4 Mar. 2021	2.2 (1.3)	80.4	60.1%	1.1%

3.2 Ultra-Rapid Neutron Only Simulation

To verify CRNS SWE estimates at the CARC, where traditional snow monitoring data does not exist, this study will utilize neutron transport modelling. Recently, CRNS studies have adopted the use of the Ultra Rapid Neutron-Only Simulation (URANOS), such as Brogi et al. (2022), Schattan et al. (2017), and Schrön et al. (2023). URANOS utilizes a Monte Carlo approach to simulate the neutrons and has been specifically developed for CRNS applications (Köhli et al., 2023). Millions of neutrons are generated from randomly distributed point sources within a user-defined area, and neutrons' path and interactions are tracked from its source to the point of detection through a ray-casting algorithm (Brogi et al., 2022; Köhli et al., 2023). URANOS can model 3-dimensional voxel-based geometries with defined materials by stacking multiple layers of either ASCII matrices or bitmap images to replicate important site characteristics (Köhli et al., 2023). For this analysis, we used URANOS v1.23, which is freely available for download at: https://gitlab.com/mkoehli/uranos/.

We ran URANOS simulations for the eight dates corresponding to the UAV lidar flights at the CARC, similar to the simulations described in Woodley et al. (2024). Our methods have two main differences from the URANOS simulations used in the Woodley et al. (2024) analysis. First, we moved the CRNS around our research domain to test how neutron counts would have been affected by the

https://doi.org/10.5194/egusphere-2025-31
Preprint. Discussion started: 27 January 2025

differing snow cover conditions around the CARC. A cylindrical virtual CRNS detector was placed at each of the 26 points on Fig. 3b roughly 2 m above the ground in URANOS. Each URANOS run simulated 10^8 neutrons. The virtual CRNS was enlarged to a 9 m radius to improve detection statistics and supplied with a detector response function (provided in the URANOS GitLab repository) to simulate the sensitivity of the CRNS installed at the CARC, specifically a high-density polyethylene moderator of 25 mm thickness. To minimize the influence of soil heterogeneity and focus on the influence of snow variability, we chose to create a uniform 30 cm soil layer with the average of all soil measurements. Soil samples for soil moisture and bulk density were collected at 5 cm depth intervals up to a total depth of 30 cm and at six cardinal directions at three different radii (approximately 25 m, 75 m, and 200 m) from the CRNS instrument (Woodley et al., 2024). Because this analysis moves the simulated CRNS instrument around the CARC where other soil moisture measurements were not made, we chose to average the soil measurements for our uniform soil layer. As in Woodley et al. (2024), soil moisture, atmospheric pressure, and other important parameters listed in Table 2 were kept constant to allow direct comparisons of model simulations due to changes in snow distribution, and to remove the need to correct counts based on differing hydrogen pools.

Table 2: Atmospheric and soil parameters used in our URANOS simulations. These values were unchanged from each set of heterogeneous and uniform snow runs.

Parameter	Value
Number of Neutrons [-]	100000000
Air Humidity [g m^{-3}]	3.341
Atmosphere Depth [g cm^{-3}]	888.809
Soil Moisture (top 30 cm) [%]	21%
Soil Bulk Density (top 30 cm) [g m^{-3}]	1.087
Soil Porosity (top 30 cm) [%]	56%

https://doi.org/10.5194/egusphere-2025-31
Preprint. Discussion started: 27 January 2025

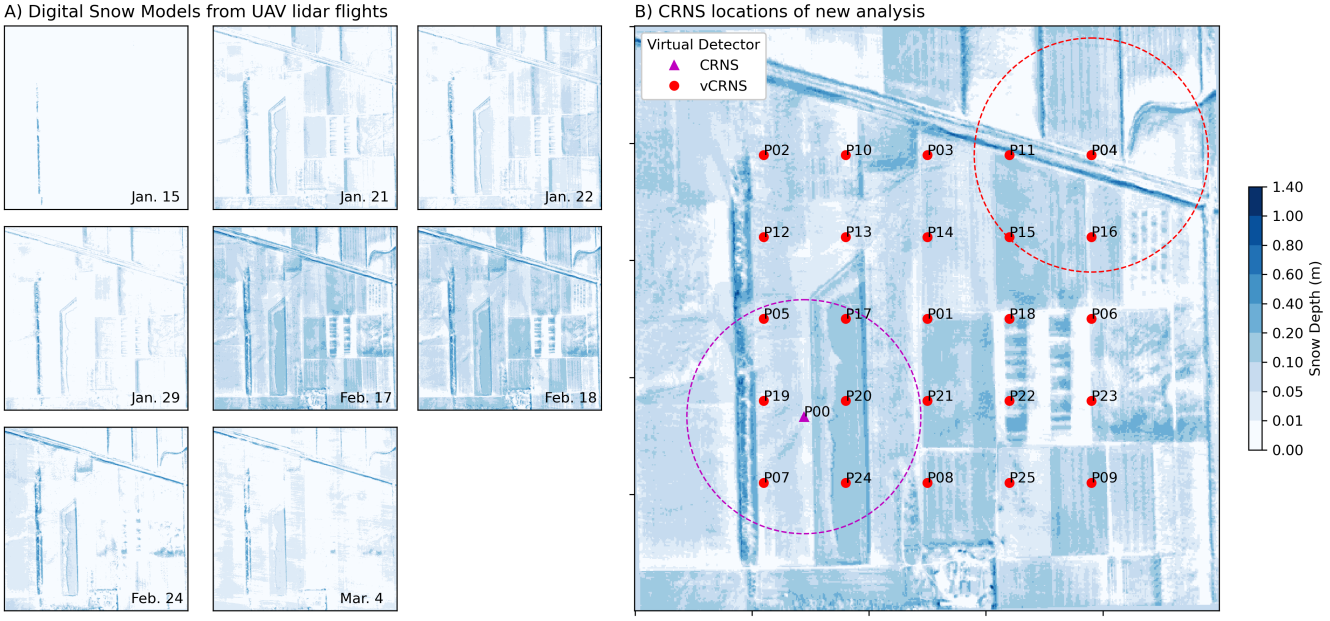

Figure 3: a) Lidar digital snow maps (DSM) from the winter 2020-2021 NASA SnowEx Prairie Mission. Colormaps for snow are not linear. Smaller increments were included to show where extremely shallow snow is located at the CARC. b) Map of locations of virtual CRNS points for URANOS simulations. The actual CRNS location is marked by the magenta triangle, with the calculated 171 m operational footprint (magenta dotted circle) of the CRNS from Woodley et al. (2024). The rest of the virtual CRNS locations used in this analysis are marked by red circles.

To examine how CRNS measurements change with the spatial distribution of snow, we ran simulations in URANOS using 1) a uniform snow layer and compared them against simulations using 2) the heterogeneous snow maps derived from the UAV lidar and snow density. For the uniform simulations, a chosen volume of snow water was evenly distributed in the research area, creating a uniform snow layer. We created two uniform snow layer schemes based off: a) the average amount of snow water in the 171 m operational footprint around the CRNS detector and b) the average amount of snow water across the entire 1 km^2 study domain. The 171 m operational footprint of the CRNS is a site-specific value calculated at the CARC using "no snow" URANOS simulations from Woodley et al. (2024). The total amount of snow water volume was divided using one of the snow density material values in URANOS. Depending on the amount of snow water per pixel, we chose to model the snowpack using the built-in material codes for snow: 240, 241, and 242, which has density values of 0.03 g cm^{-3}, 0.1 g cm^{-3}, 0.3 g cm^{-3}, respectively, to create a snow layer with uniform thickness and density (see MaterialCodes.txt in GitLab repository, link in Sect. 3.2).

From the different URANOS simulations, we also calculated SWE from the modelled neutron counts. We followed our methods from Woodley et al. (2024) to calculate modelled SWE from URANOS. SWE calculations were made using Eq. (1) (Desilets, 2017) using our modelled neutron counts from URANOS simulations.

$$\mathrm{SWE} = -\Lambda \ln \frac{N - N_{wat}}{N_\theta - N_{wat}} \quad (1)$$

N_θ is the calibration neutron count, from the "snow-off" reference date of 15 January 2021. N is the neutron counts corresponding to the dates of the subsequent seven "snow-on" lidar flights at the CARC

https://doi.org/10.5194/egusphere-2025-31
Preprint. Discussion started: 27 January 2025

(21 Jan. 2021 to 4 Mar. 2021). The attenuation length (Λ) was calculated to be 4.8 cm from previous literature (Desilets et al., 2010). N_{wat} is the counting rate over an infinite depth of water and can be calculated using Eq. (2):

$$\mathrm{N_{wat}} = 0.24\mathrm{N_0} \tag{2}$$

where 0.24 is an assigned constant value (Desilets, 2017; Desilets et al., 2010). N_0 is the theoretical counting rate over dry soils:

$$N_0 = \frac{N_\theta}{\frac{a_0}{\theta_g \rho_{bd} + a_2} + a_1} \tag{3}$$

where $a_0 = 0.0808$, $a_1 = 0.372$, and $a_2 = 0.115$ (Desilets et al., 2010; Desilets, 2017). Usually, N_θ in Eq. (3) is multiplied by a correction factor, $F(t)$, to correct for solar activity, atmospheric pressure, and humidity. However, as all our model simulations used the exact same meteorologic conditions, our correction factor was set to 1. θ_g is the gravimetric soil water content and ρ_{bd} is the soil bulk density, which were obtained from in situ soil samples.

3.3 Comparisons with Gridded SWE Products

To evaluate whether CRNS SWE has potential value for future remote sensing missions or gridded datasets, we compared our CRNS SWE and UAV lidar SWE to several available gridded SWE products at several spatial resolutions. We chose the Western United States UCLA Daily Snow Reanalysis (hereafter UCLA-re, ~500 m resolution, Fang et al., 2022), the Snow Data Assimilation System (SNODAS, 1 km resolution, National Operational Hydrologic Remote Sensing Center, 2004) from National Oceanic and Atmospheric Administration's National Weather Service National Operational Hydrologic Remote Sensing Center, and the Daily 4 km Gridded SWE (hereafter UA, 4 km resolution, Broxton et al., 2019) from the University of Arizona.

The UCLA-re dataset is generated from assimilation data with Landsat fractional snow cover area and other input data such as meteorological forcings from the Modern-Era Retrospective analysis for Research and Applications, version 2 (MERRA-2) (Margulis et al., 2019). A Bayesian analysis is performed on prior estimates of snow states and fluxes using a land surface model and snow depletion curves (Margulis et al., 2019). SNODAS provides daily gridded estimates of SWE for the conterminous United States by utilizing a snow model, which is forced by downscaled numerical weather predictions (Clow et al., 2012). Digitally available airborne, satellite, and ground-based snow data are then assimilated into the model to provide a best estimate of near real-time snow estimates (Clow et al., 2012; Driscoll et al., 2017). The UA dataset provides SWE and snow depth estimates by assimilating snow station data such as the snow telemetry (SNOTEL) network and precipitation and temperature data using the gridded PRISM model (Zeng et al., 2018). For each gridded dataset, we chose the pixel that included the CARC. Only the SWE for the UCLA-re data was aggregated and averaged within a 2-pixel by 2-pixel region, to obtain an area that is like the 1 km^2 area of the CARC. All gridded datasets are freely available for download at the National Snow and Ice Data Center (last accessed: 3 October 2024).

https://doi.org/10.5194/egusphere-2025-31
Preprint. Discussion started: 27 January 2025

4 Results and Discussion

4.1 Neutron Modelling

Figure 4 shows the differences between heterogeneous runs (i.e., spatially varying snow distribution derived from the UAV lidar and snow density) and the uniform runs (i.e., uniform snow distribution) from 15 January 2021, to isolate the effects of large snow drifts on CRNS measurements. Each point in Fig. 4a represents a different virtual CRNS location within our study domain (shown in Fig. 3b). On this date, most of the CARC was uncovered except for some isolated patches of extremely shallow snow and a large snowdrift in the southwest corner of the study domain (top left panel of Fig. 3a, and Fig. 4b). Most virtual CRNS locations resulted in neutron counts from the heterogenous and uniform runs that were within 1% of error from each other. However, points P00, P05, P07 and P19 yielded large differences of greater than 100 neutrons (approximately 3% error). These four points are also the closest to the snow drift on 15 January 2021 (see Fig. 4b).

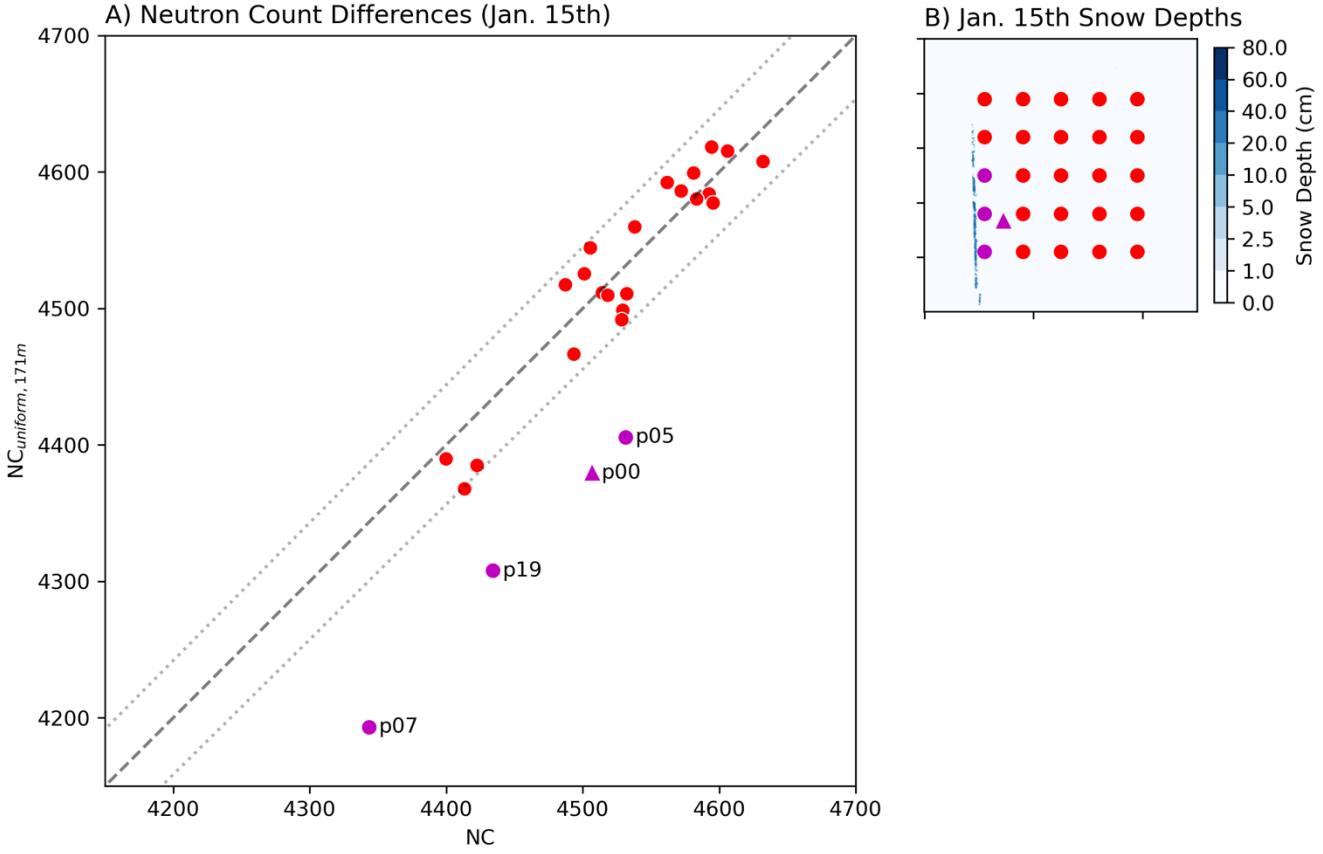

Figure 4: a) A scatterplot comparing neutron counts from the uniform runs (y-axis) against the heterogeneous runs (x-axis) for 15 January 2021, the near-no-snow baseline, with the exception being the large north-south snow drift in the western portion of the study area. While most points fell near the one-to-one line (black dashed line) and within a 1% error, four virtual CRNS locations yielded large differences in neutron counts: P00, P05, P07, and P19. b) Map of the snow depth from the 15 January 2021 UAV lidar flight, shown in the colorbar. The snow drift is the slim blue linear feature on the left (western) portion of the study area. The

https://doi.org/10.5194/egusphere-2025-31
Preprint. Discussion started: 27 January 2025

virtual CRNS locations in URANOS are shown in circles, while the actual CRNS location from winter 2020-2021 is shown in a triangle (as in Fig. 3b). The four points with the largest neutron count differences are marked in magenta.

Figure 5 compares how the neutron counts change with relation to the snowpack variability, where the neutron model domain was divided into twelve sectors of equal angle from the virtual CRNS detector. We noticed skews in neutron origins due to the relation of the model geometry, namely the position of the virtual detector and the source geometry. Virtual detectors placed closer to the edges of our domain had neutron origins that were skewed towards the centre of the domain. Therefore, we limited the neutron counts in the sectors to a 200 m radius. The radial plots in Fig. 5 shows the percent change in neutron counts from the uniform runs in each sector on 15 January. P07 (Fig. 5a) saw the biggest percent change between the no-snow (right of N-S line) and snow side (left of N-S line) with an average percent change of 5% in neutron counts compared to 1.6% change, respectively. We observed a similar but smaller trend in P05 (Fig. 5c) with an average 3.16% change on the no-snow side and 2.3% change on the snow side. In both P19 (not shown) and P00 (Fig. 5b), we observed larger changes on the snow side compared to the no-snow side. P00 had a 5.3% change on the snow side compared to a 2.4% change on the no-snow side. P19 had a 3.9% change on the snow side and a 2.1% change on the no-snow side. The differences in P00 neutron counts are likely explained by the longer distance away from the snow drift (Fig, 5e). Many studies have shown that CRNS is extremely sensitive to its immediate surroundings (Köhli et al., 2015; Schrön et al., 2017). The removal of snow cover around the CRNS from the uniform run is likely to have a larger effect on neutron counts than the snow drift. P05, P07, and P19 which were modelled closer to the snow drift. The differences are likely caused by the breaks in the snow drift as it first formed. P07 (Fig. 5d) was placed next to a longer, contiguous section of the snow drift compared to P05 (Fig. 5f), which enhances the neutron counts on the snow side in the heterogeneous runs. We observed similar breaks in P19.

https://doi.org/10.5194/egusphere-2025-31
Preprint. Discussion started: 27 January 2025

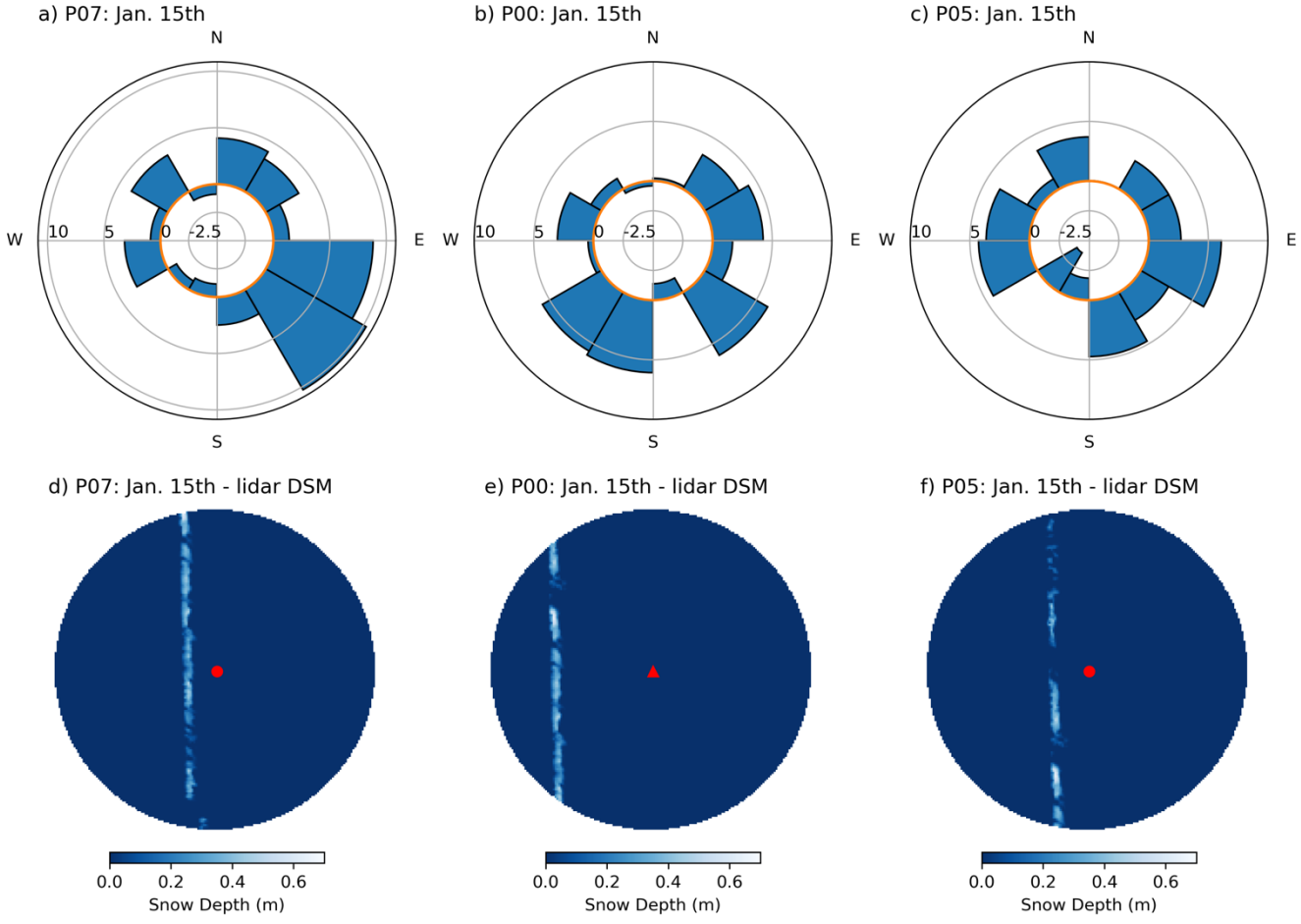

Figure 5: Percent changes in neutron counts of the heterogenous runs from the uniform runs for 12 sectors around the virtual CRNS location for the 3 out of the 4 points identified in Fig. 3: a) P07, b) P00, and c) P05. The orange line on panels a-c marks no change in neutrons counts in the heterogeneous runs from the uniform runs. The snow distribution on 15 January 2021 is shown for each point on panels d-f to contextualize the differences.

Figure 6 shows the difference in neutron counts (Fig. 6a) and SWE (Fig. 6b) estimates between the heterogeneous and uniform URANOS results for the rest of the other dates. In this case, the uniform runs use the average SWE within the nominal 171m radius footprint around each virtual CRNS. Neutron counts are biased higher in the heterogeneous runs with a mean bias percent error (MBPE) of 1.8% and a root mean squared percent error (RMSPE) of 2.6%. When we calculate the SWE using these URANOS runs and Equation 1, SWE would be overpredicted in the uniform runs with an MBPE = 19.6% and a RMSPE = 34.9% cm. We grouped the errors across all dates by their points, to determine which points had the largest and smallest errors in neutron counts (Fig. 6c). The largest differences were found in Points P00, P05, P19, and P03. Points P00, P05, and P19 are again the 3 closest points to the large snow drift in the western portion of the study area. P03 (top row, center in Fig. 3b) is also located near snow drifts that formed due to topographical changes near train tracks that cross the CARC. The lowest errors were found in Points P17, P15, P24 and P06. The commonality between points P17, P15,

https://doi.org/10.5194/egusphere-2025-31
Preprint. Discussion started: 27 January 2025

P24, and P06 were likely relatively uniform snow cover surrounding the virtual CRNS for most of the dates. P17 and P24 were in the same field directly to the left of P00, which had relatively uniform snow trapped from the field around most of the dates during winter 2020-2021. P00, P05, P19, and P03 had much more variable snow cover surrounding the virtual CRNS, with the large snow drift on one side and bare ground on the other for most dates in winter 2020-2021.

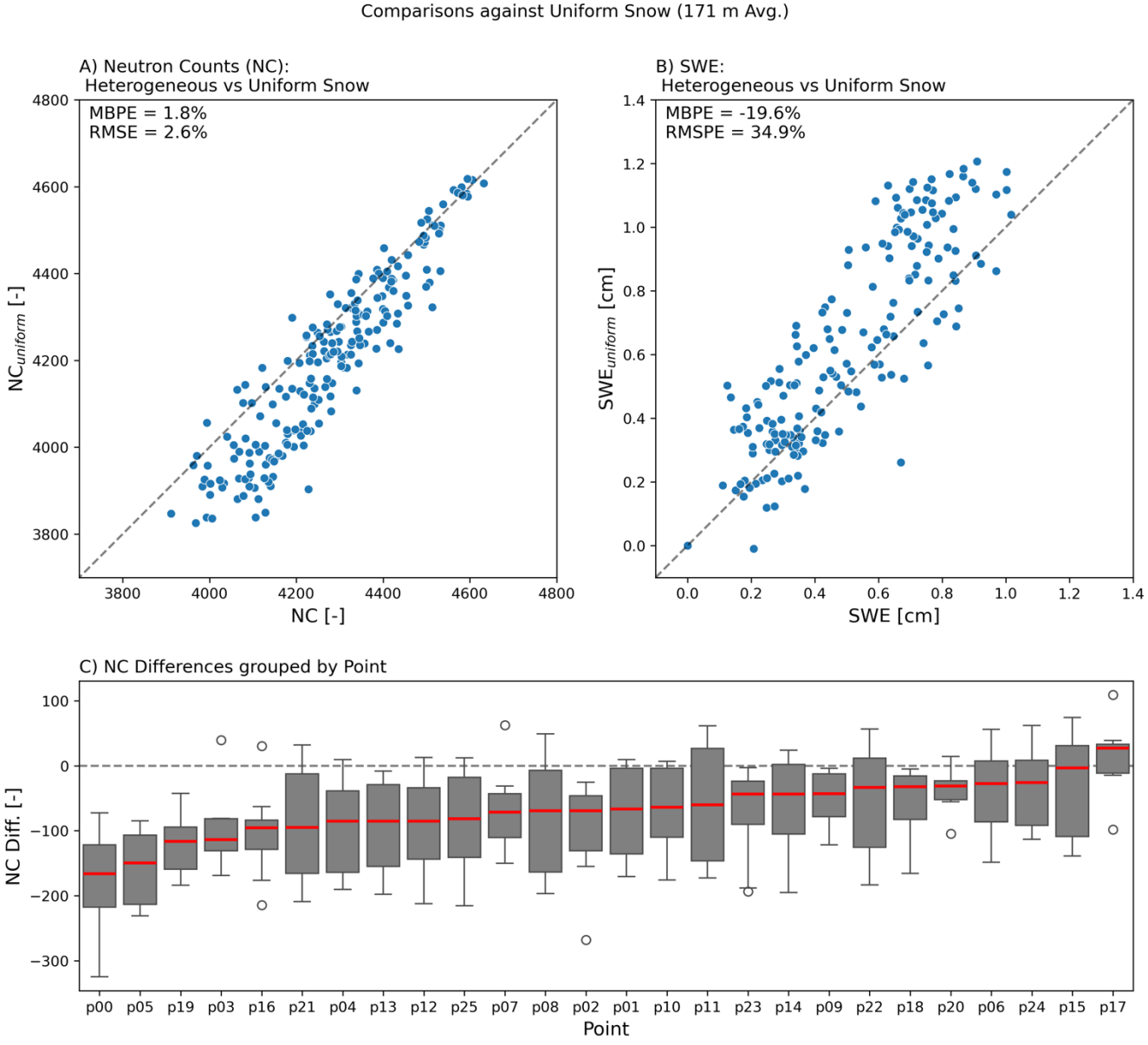

Figure 6: Scatterplot comparing a) neutron counts and b) SWE for the heterogenous snow runs (x-axis) against uniform snow runs (y-axis) that use the average SWE of the 171 m radius footprint surrounding the virtual. c) Boxplots showing the difference between the heterogenous and uniform snow runs for each virtual CRNS location (show in Figure 3b), where each box contains the eight URANOS simulations corresponding to the UAV lidar flights at the CARC.

https://doi.org/10.5194/egusphere-2025-31
Preprint. Discussion started: 27 January 2025

Figure 6 also demonstrates the need to accurately measure and map where the snow is distributed, especially for a shallow heterogeneous snowpack. One might assume that neutron counts between these two runs should be comparable because both have the same total snow water volume within the operation footprint of the CRNS. However, the distribution of that snow water is different between the two runs. Differences will account for the various patches of bare ground or snow drifts that formed around the CARC due to snow redistribution among fallow fields, crop stubble, and shelter belts. Figure 6c suggests that snow drifts closer to the CRNS bias neutron counts the most, leading to the largest differences in neutron counts compared to a uniform snow scenario.

Correlation analysis (not shown) also suggests that snow drifts are the biggest contributors to neutron count variability at our study site. For all points and dates, differences in neutron counts between the heterogeneous and uniform snow runs (hereafter ΔNC_f) were positively correlated with statistical significance ($r = 0.451$) with the percentage of bare ground within the operation footprint of the CRNS. The percentage of bare ground in the operation footprint was calculated by cropping the UAV lidar snow depth to a circular area within 171 m from the virtual CRNS location and finding the percentage of bare ground within the masked area. ΔNC_f closer to 0 were found when the percent of bare ground in the CRNS footprint was closer to 100%, suggesting that bare ground did not lead to reduced neutron counts. In heterogeneous snow environments like the CARC, it suggests that the tall snow drifts, especially within proximity of the CRNS, are creating the biggest changes in neutron counts. Statistically significant negative correlations were found when comparing variability of snow depths – namely the standard deviation and the range (difference in max. and min. snow depths) - within the CRNS footprint and ΔNC_f (-0.66 with standard deviations and -0.566 with range). Taking the same correlations after grouping our measurements by points, we still observe statistically significant negative correlations for the median standard deviations and median range of footprint snow depths with respect to the median ΔNC_f (-0.643 and -0.582 respectively). The median bare ground percent within the CRNS footprint were neither correlated (0.107) nor statistically significant with ΔNC_f. Interestingly, this suggests our actual CRNS location for winter 2020-2021 was somewhat biased, especially towards 17 and 18 February 2021.

Figure 7 shows similar trends comparing the heterogeneous runs with the uniform runs using the average SWE of the entire 1 km^2 CARC study domain (as opposed to the average SWE in the 171 m radius surrounding the virtual CRNS). The variability of the difference between the heterogenous and uniform snow runs increased for both neutron counts (Fig. 7a) and SWE (Fig. 7b) using the CARC average instead of the CRNS footprint average. Neutron counts were biased towards the heterogeneous runs with an MBPE of 1.9% and an RMSPE of 3.1% and SWE were biased towards the uniform runs with an MBPE of -22.9% and a RMSPE = 42.3%. This greater variability is expected due to the fact that more neutrons detected by the CRNS originate near the instrument as opposed to far away, so the SWE in the surrounding area has a greater influence on the neutron counts than in more distant areas. Most applications of CRNS will likely be to characterize the areal average SWE. Comparing the heterogeneous runs to the CARC average SWE runs allows us to evaluate which virtual CRNS locations were most reflective of the CARC average. The points that were most reflective of the CARC average were points p20, p07, p06, and p19. Interestingly, points p20, p07, and p19 are the three points clustered around the actual CRNS instrument at the CARC. P06 was not located near the original CRNS but had some snow cover through most of January and February. Points 13, 14, and 10 were also similarly

https://doi.org/10.5194/egusphere-2025-31
Preprint. Discussion started: 27 January 2025

clustered close together (NW quadrant) closer to the train track snow drifts. We theorize that at times these points sampled too many snow drifts or too little snow during the winter.

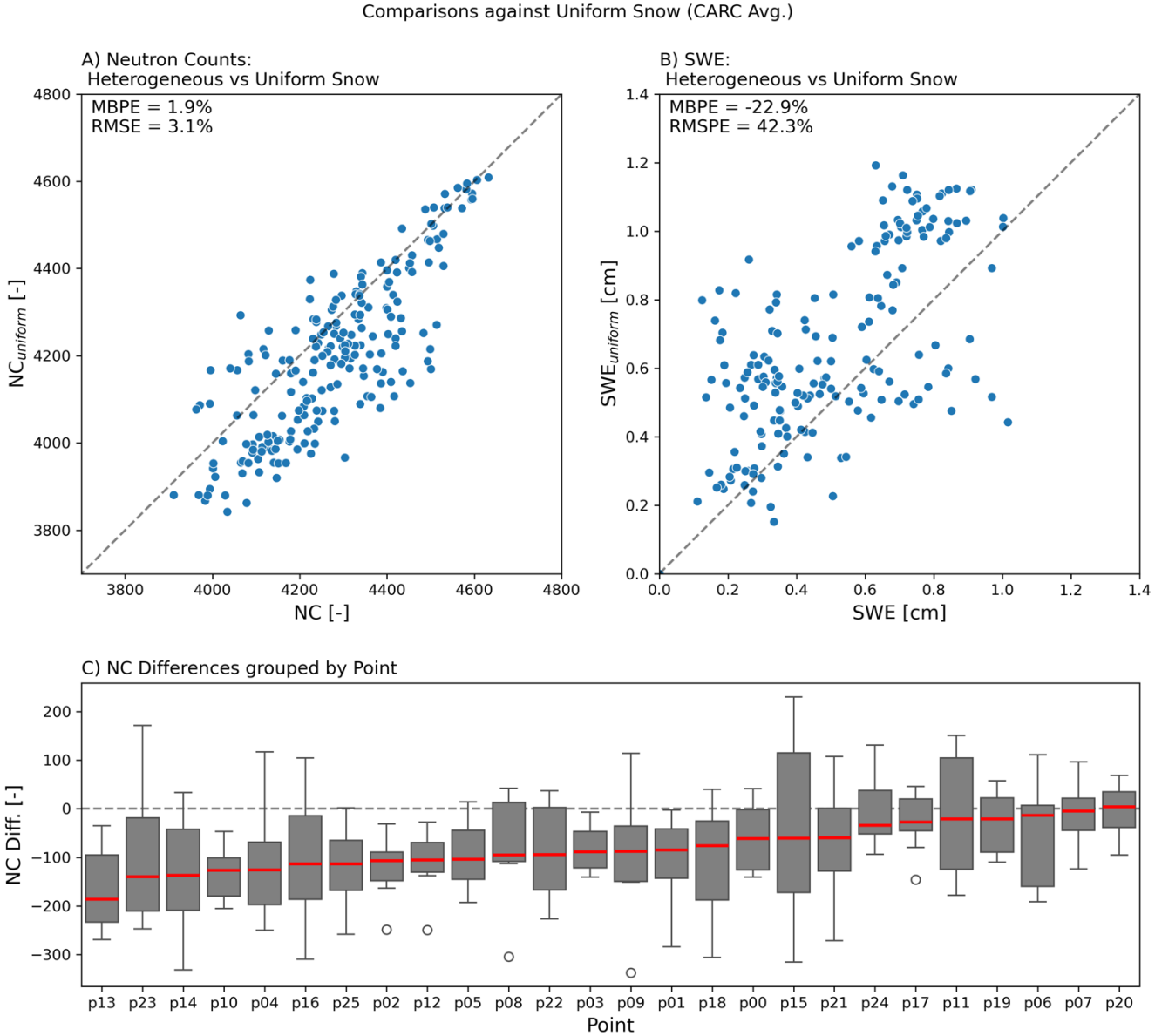

Figure 7: Same is Fig. 6 but for uniform snow created from the 1 km² CARC average.

4.2 CRNS Spatial Representativeness

In this work, we executed 624 separate URANOS neutron transport simulations for the CARC study area in order to understand the influence of spatial variability on CRNS observations. To supplement these findings, we conducted a secondary analysis to evaluate the spatial representativeness of CRNS SWE at our prairie site compared to the observations that might have been collected from a more

https://doi.org/10.5194/egusphere-2025-31
Preprint. Discussion started: 27 January 2025

traditional snow scale SWE instrument. In most cases, CRNS or other SWE instruments would be deployed in hopes of capturing the average snow conditions representative of a large area. To do this, we averaged the lidar-derived SWE DSMs for each of the eight UAV flights to 1 m^2 spatial resolution. We calculated the kernel density of all of these 1 m^2 SWE pixels to understand the full distribution of SWE across the study site, where each pixel represents a possible SWE measurement that could have been collected by a naively located snow scale or snow pillow (of measurement area equal to 1 m^2). Then, we applied the CRNS spatial weighting function from Woodley et al. (2024) to each of these pixel locations (actually, every 4th pixel to increase computational efficiency), using a wraparound boundary to remove edge effects from pixels close to the boundary of the study site. This allowed us to retrieve a distribution of synthetic CRNS SWE estimates across the entire CARC.

We acknowledge that this analysis is naive in that it assumes that the CRNS spatial weighting function would be constant across the entire study site. In reality, the spatial sensitivity of CRNS can change with snow spatial distribution and magnitude, and soil moisture distribution and magnitude, among other factors. The wraparound boundary also means that none of the CRNS SWE estimates from this analysis, especially those near the boundaries of the study area, are truly reflective of the "true" SWE that would be observed by CRNS at the same location within the site.

However, it does mean that each CRNS SWE estimate is derived from the same lidar-derived SWE data, which reflects a spatial snow distribution representative of a prairie site. Lastly, this analysis assumes that a snow scale or snow pillow would exactly measure the SWE in each given location. However, this is unlikely to be true given that snow will likely accumulate differently on a smooth artificial surface versus the natural ground surface, especially in the windy, shallow snow conditions typical of the prairie. In summary, this analysis is not as rigorous in reproducing CRNS behavior as the URANOS simulations presented above. Still, it does provide a first-order estimate of the spatial representativeness of CRNS SWE estimates at a prairie site versus more conventional, smaller-footprint SWE instruments.

Figure 8a shows the kernel density distribution of synthetic SWE estimates from the CRNS locations across the entire CARC (blue), compared to the distribution of 1 m^2 lidar-derived SWE pixels from the entire CARC (red) for an example date of 29 January 2021. This date was more than one week after the most recent snow event, allowing for wind redistribution, sublimation, and potentially melting of the snow during the intervening period. The spatial average lidar-derived SWE for the entire CARC is shown in the vertical, black dashed line. A similar plot is shown in Fig. 8b for 17 February 2021, soon after a large snow event (and the most pronounced snowpack of the season). In both cases, the

https://doi.org/10.5194/egusphere-2025-31
Preprint. Discussion started: 27 January 2025

CRNS SWE distribution is shifted closer to the CARC average, compared to the 1 m^2 SWE distribution.

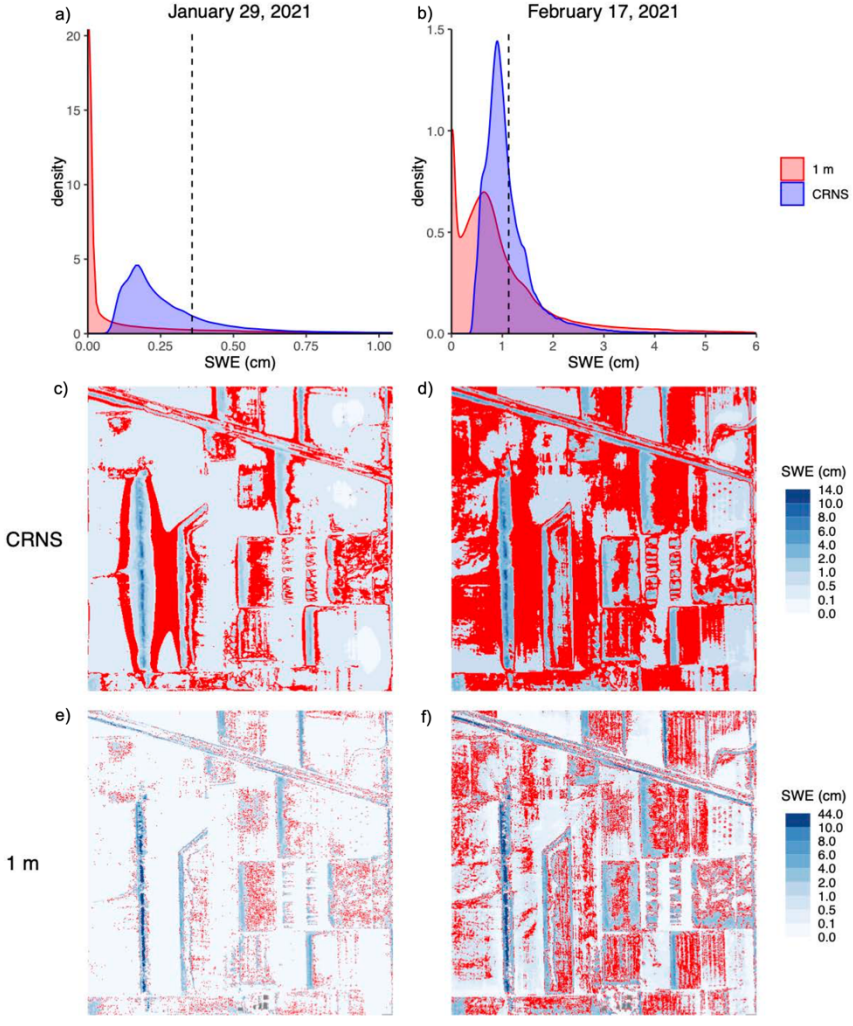

Figure 8: Simulation of the spatial representativeness of a synthetic aboveground CRNS at the CARC versus a synthetic snow scale or pillow of area 1m^2. a) and b) Probability density functions of the SWE observed by CRNS (blue) versus a synthetic snow scale or pillow of pixel size 1m by 1m (red) for 29 January and 17 February 2021, respectively. The vertical dashed line shows the mean SWE of the entire study 1 km^2 area. It is evident on both dates that the probability density of CRNS SWE estimates is shifted closer to the areal mean. c) and e) show the areas where the CRNS and 1m pixels are within +/- 25% of the mean SWE of the entire study area, respectively, for 29 January 2021. The red pixels are locations that are within +/- 25% of the areal mean SWE, while the underlying blue color map shows the SWE magnitude. d) and f) show the same information for 17 February 2021. Generally, the CRNS is representative of a larger proportion of the study area and the representative areas are more contiguous, compared to the 1m resolution synthetic snow scale or pillow.

For 29 January, the CARC average SWE was 0.4 cm. 23% of the CRNS locations were within +/- 25% of the CARC average, while only 5% of the 1m^2 pixels were within that same range. For February 17, the CARC average SWE was 1.1 cm, and 50% of the CRNS locations and 20% of the 1m^2 pixels were within +/- 25% of the CARC average, respectively. Across all dates (excluding January 15,

https://doi.org/10.5194/egusphere-2025-31
Preprint. Discussion started: 27 January 2025

2021, which had very spatially limited snow cover), this analysis indicated that the percentage of the CARC study area for which a CRNS would return a SWE estimate within +/- 25% of the CARC average ranged from 21%-50%, while the 1 m^2 pixels ranged from 5%-20% of the CARC. In summary, our first-order analysis indicated that a naively sited CRNS was 2.3 to 5 times more likely to return a SWE estimate within +/- 25% of the large-scale spatial average than a similarly sited SWE sensor with a footprint of 1 m^2.

These results are shown spatially in Fig. 8 c&e, where 8c shows the map of CRNS SWE estimates, and 8e shows the lidar-derived SWE at 1 m^2 resolution for the example date of 29 January 2021. In both maps, locations that returned a SWE value within +/- 25% of the CARC average are shown in red. The representative areas for CRNS are more extensive and spatially contiguous, while the representative 1 m^2 pixels are fewer and less spatially contiguous. The same maps are shown for 17 February 2021 in Figs. 8 d&f. In this case, a larger proportion of the CARC is representative of the large-scale CARC average in both maps, and the CRNS similarly shows more extensive and more contiguous representative areas. These results indicate that CRNS provides value for large-scale SWE estimates in the prairies, beyond those available from more conventional, smaller-footprint sensors. It appears that the optimal locations to site CRNS in prairie snow distributions like the CARC are in locations of low snow accumulation near areas of high snow accumulations (e.g. snow drifts). This makes sense, as most of the CARC area exhibits low snow accumulation, while only a small portion experiences higher snow accumulation, and CRNS are most sensitive to the area immediately surrounding the instrument. Through a combination of design and happenstance, our actual CRNS at the CARC (point P00 on Fig. 3) is located within a representative region for all lidar dates (with the exception of 15 January 2021, which had very spatially limited snow cover).

4.3 Comparison against Gridded SWE Estimates

Figure 9 shows comparisons of SWE (Fig. 9a) and snow depth (Fig. 9b) products at similar magnitudes of scale (see Sect. 3.3 for details). We also plotted our CRNS SWE time series at the CARC from Woodley et al., (2024). In January and March 2021, all gridded SWE products had no SWE. This contrasts with the average CARC SWE from the UAV lidar DSMs (red squares on Fig. 9a) and CRNS simulations (grey boxplots on Fig. 9a), and our CRNS SWE times series (green line, Fig. 9a), where snow cover is still present on the ground. In February, the UCLA Snow Reanalysis and SNODAS predicted more peak SWE on the 17th and 18th of February 2021 compared to our average CARC SWE, with SNODAS almost double our CARC SWE estimates. The UA SWE produced similar estimates to our CARC SWE in mid-February, before predicting more SWE in late-February and underpredicting SWE starting in March.

https://doi.org/10.5194/egusphere-2025-31
Preprint. Discussion started: 27 January 2025

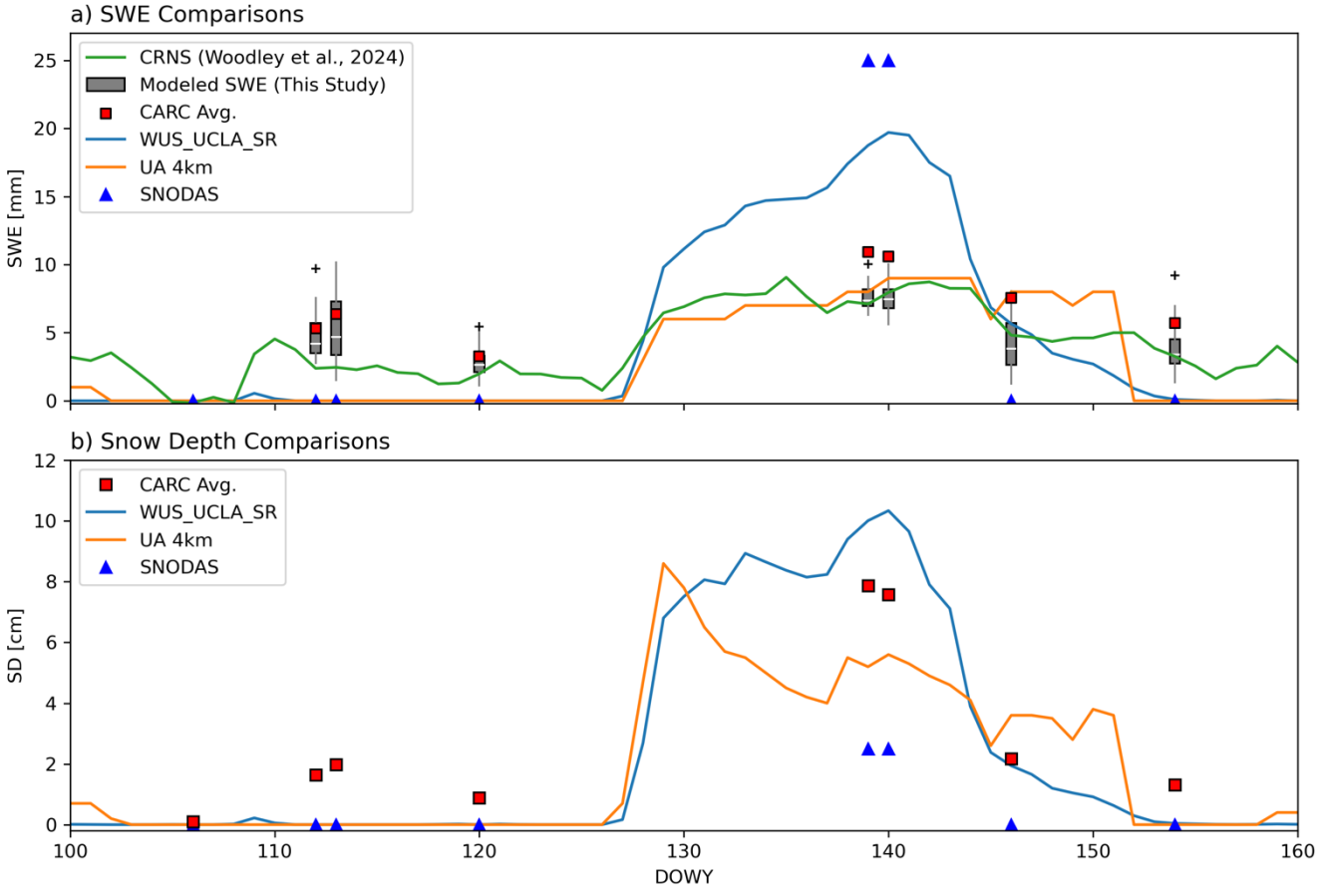

Figure 9: Comparisons of SWE estimates of a) gridded SWE and in situ SWE estimates and products for January to March 2021 and b) snow depth products expressed as the day of water year (DOWY; days after 1 October 2020). A time series of the UCLA Snow Reanalysis (blue line), UA SWE (orange line), CRNS (green line) from Woodley et al., (2024) are shown. Only the UCLA Snow Reanalysis and UA datasets are shown for snow depths. Daily SNODAS SWE and snow depth estimates for each of the dates corresponding to a lidar flight are shown as blue triangles, and an averaged CARC SWE and snow depth for each digital snow model (DSM) for the 1 km^2 study region are plotted as red squares. Modelled SWE estimates from this study for each date are plotted as grey boxplots to illustrate the variability of SWE within our study region.

The differences in SWE products are likely due to aggregation with different resolution and meteorological forcings. The sub-grid variability is shown to be very important in estimating the SWE in a prairie environment, where the average SWE is either grossly under or overpredicted. Past studies have indicated that SNODAS is unsuccessful at capturing the spatial variability in regions with persistent winds like the prairies (Lv et al., 2019). We also verified that similar issues occur with snow depths. Figure 9b plots a similar graph, except showing the changes in snow depths for the parts of January to March 2021. Snow depths show a similar pattern, where there are no snow depths in the gridded datasets in January 2021 and March 2021, and snow depths detected for February 2021. SNODAS underestimates the snow depths compared to our average CARC SWE, despite having similar spatial resolution (1 km for SNODAS and a 1 km aggregate for lidar CARC SWE).

https://doi.org/10.5194/egusphere-2025-31
Preprint. Discussion started: 27 January 2025

While Fig. 9a shows that SWE estimates from the UA 4km data are more reliable in February 2021, Fig. 9b suggests the UCLA-re snow depths are more reliable estimates compared to the average CARC snow depths. This suggests snow density estimates in the UCLA-re are overpredicted. No gridded product produced non-zero snow depths or SWE in January 2021, despite snow being present as shown by our lidar and CRNS measurements. The timing of precipitation from all three models also does not seem to line up with some of our in-situ measurements. UCLA-re shows a brief precipitation event between the 15 January 2021 UAV flight and the 21 January 2021 UAV flight, and coincident with a known snowfall event between 18-19 January 2021 (see Supporting Information for Woodley et al. (2024)). However, snow disappears quickly after the snowfall event. Lower estimates of mean SWE and SD are expected for larger spatial resolutions due to increased aggregation (Blöschl, 1999).

Our analysis shows CRNS has utility for improving SWE estimates in prairie environments, and other environments with shallow, heterogeneous snowpacks. CRNS measurements have already shown this utility in mountain regions. Integration of CRNS SWE into models, alongside remote sensing data, has reduced error spread in the Austrian Alps (Schattan et al., 2020). CRNS has the potential to increase the coverage of SWE monitoring sites, where currently used technologies within snow monitoring networks like SNOTEL may not be optimal in the northern Great Plains. Previous research has shown that large errors in SWE were due to subpixel SWE variability of the Northern Great Plains (Tuttle et al., 2018). However, we hope that future planned satellite missions such as NISAR, armed with similar instrumentation used in the CARC during SnowEx 2021 (Palomaki and Sproles, 2023) can improve efforts to monitor snow in this relatively under-instrumented region.

5 Conclusions

A neutron transport modelling study at an agricultural site in the Northern Great Plains of Montana has shown that the spatial variability of shallow and heterogeneous snowpack affects CRNS measurements. While bare ground effects have been shown in other studies, the amount of snow heterogeneity in semi-arid prairie environments suggests that the location and magnitude of snow drifts have a larger effect on neutron counts. Comparisons with gridded SWE products shows CRNS has the potential to improve estimates, when compared to lidar-derived SWE from the site. The snow distribution should be considered when siting aboveground CRNS instruments in areas of high snow spatial heterogeneity, even for very shallow snowpack like that at the CARC, if the goal is for the instrument to be representative of the large-scale spatial average. Our analysis suggests that CRNS instruments should be placed in areas of low snow accumulation that are nearby higher snow accumulation areas. However, a naively sited CRNS instrument (i.e., with no knowledge of the snow distribution) is still 2 to 5 times more likely to be representative of the large-scale average SWE than a more conventional, smaller footprint SWE sensor such as a snow scale or snow pillow. Our study focuses solely on the effect of snow distribution on CRNS, but spatial variability of soil moisture is also important to consider, especially in shallow snowpack areas such as the prairie where the effect of soil moisture distribution on CRNS measurements may be of comparable magnitude to that of snow distribution. This highlights the need for further research in semi-arid prairie environments like the northern Great Plains.

https://doi.org/10.5194/egusphere-2025-31
Preprint. Discussion started: 27 January 2025

Code and Data Availability

Code and data used in this analysis will be made available through GitHub at https://github.com/heyjoekim/spatial_crns_carc and archived on Zenodo at https://doi.org/10.5281/zenodo.14592408.

Author Contribution

HK did the formal analysis and wrote the initial draft of the research conceptualized by ST and HK. ES installed the CRNS and completed the drone flights at the CARC. ST and ES reviewed and edited the paper.

Competing interests

The contact author has declared that none of the authors has any competing interests.

Acknowledgements

We would like to acknowledge the partial funding we received from the National Aeronautics and Space Administration (NASA) Terrestrial Hydrology Program for their support of this field campaign. We would also like to Thank Dr. Eric Sproles' graduate and undergraduate students for their participation for their participation in the ground-based snow sampling during winter 2020-2021. We would also like to thank Dr. Markus Köhli and Dr. Cosimo Brogi for their help in understanding how to operate and set up the URANOS simulations used in this study.

References

Aase, J. K. and Siddoway, F. H.: Stubble height effects on seasonal microclimate, water balance, and plant development of no-till winter wheat, Agricultural Meteorology, 21, 1–20, https://doi.org/10.1016/0002-1571(80)90065-5, 1980.

Bales, R. C., Molotch, N. P., Painter, T. H., Dettinger, M. D., Rice, R., and Dozier, J.: Mountain hydrology of the western United States, Water Resour. Res., 42, https://doi.org/10.1029/2005WR004387, 2006.

Baroni, G., Scheiffele, L. M., Schrön, M., Ingwersen, J., and Oswald, S. E.: Uncertainty, sensitivity and improvements in soil moisture estimation with cosmic-ray neutron sensing, Journal of Hydrology, 564, 873–887, https://doi.org/10.1016/j.jhydrol.2018.07.053, 2018.

https://doi.org/10.5194/egusphere-2025-31
Preprint. Discussion started: 27 January 2025

Blöschl, G.: Scaling issues in snow hydrology, Hydrol. Process., 13, 2149–2175, https://doi.org/10.1002/(SICI)1099-1085(199910)13:14/15<2149::AID-HYP847>3.0.CO;2-8, 1999.

Bogena, H. R., Huisman, J. A., Baatz, R., Hendricks Franssen, H.-J., and Vereecken, H.: Accuracy of the cosmic-ray soil water content probe in humid forest ecosystems: The worst case scenario: Cosmic-Ray Probe in Humid Forested Ecosystems, Water Resour. Res., 49, 5778–5791, https://doi.org/10.1002/wrcr.20463, 2013.

Brogi, C., Bogena, H. R., Köhli, M., Huisman, J. A., Hendricks Franssen, H.-J., and Dombrowski, O.: Feasibility of irrigation monitoring with cosmic-ray neutron sensors, Geosci. Instrum. Method. Data Syst., 11, 451–469, https://doi.org/10.5194/gi-11-451-2022, 2022.

Clow, D. W., Nanus, L., Verdin, K. L., and Schmidt, J.: Evaluation of SNODAS snow depth and snow water equivalent estimates for the Colorado Rocky Mountains, USA, Hydrological Processes, 26, 2583–2591, https://doi.org/10.1002/hyp.9385, 2012.

Desilets, D.: Calibrating A Non-Invasive Cosmic Ray Soil Moisture For Snow Water Equivalent, https://doi.org/10.5281/ZENODO.439105, 2017.

Desilets, D., Zreda, M., and Ferré, T. P. A.: Nature's neutron probe: Land surface hydrology at an elusive scale with cosmic rays: NATURE'S NEUTRON PROBE, Water Resour. Res., 46, https://doi.org/10.1029/2009WR008726, 2010.

Franz, T. E., Zreda, M., Rosolem, R., and Ferre, T. P. A.: A universal calibration function for determination of soil moisture with cosmic-ray neutrons, Hydrol. Earth Syst. Sci., 17, 453–460, https://doi.org/10.5194/hess-17-453-2013, 2013.

Franz, T. E., Wang, T., Avery, W., Finkenbiner, C., and Brocca, L.: Combined analysis of soil moisture measurements from roving and fixed cosmic ray neutron probes for multiscale real-time monitoring, Geophysical Research Letters, 42, 3389–3396, https://doi.org/10.1002/2015GL063963, 2015.

Gray, D. M.: Snow Hydrology of the Prairie Environment, Snow Hydrology, 21–34, 1970.

Harder, P., Pomeroy, J. W., and Helgason, W. D.: Implications of stubble management on snow hydrology and meltwater partitioning, Canadian Water Resources Journal / Revue canadienne des ressources hydriques, 44, 193–204, https://doi.org/10.1080/07011784.2019.1575774, 2019.

Iwema, J., Rosolem, R., Baatz, R., Wagener, T., and Bogena, H. R.: Investigating temporal field sampling strategies for site-specific calibration of three soil moisture–neutron intensity parameterisation methods, Hydrol. Earth Syst. Sci., 19, 3203–3216, https://doi.org/10.5194/hess-19-3203-2015, 2015.

https://doi.org/10.5194/egusphere-2025-31
Preprint. Discussion started: 27 January 2025

Köhli, M., Schrön, M., Zreda, M., Schmidt, U., Dietrich, P., and Zacharias, S.: Footprint characteristics revised for field-scale soil moisture monitoring with cosmic-ray neutrons, Water Resources Research, 51, 5772–5790, https://doi.org/10.1002/2015WR017169, 2015.

Köhli, M., Schrön, M., Zacharias, S., and Schmidt, U.: URANOS v1.0 – the Ultra Rapid Adaptable Neutron-Only Simulation for Environmental Research, Geosci. Model Dev., 16, 449–477, https://doi.org/10.5194/gmd-16-449-2023, 2023.

Kort, J., Bank, G., Pomeroy, J., and Fang, X.: Effects of shelterbelts on snow distribution and sublimation, Agroforest Syst, 86, 335–344, https://doi.org/10.1007/s10457-011-9466-4, 2012.

Lv, Z., Pomeroy, J. W., and Fang, X.: Evaluation of SNODAS Snow Water Equivalent in Western Canada and Assimilation Into a Cold Region Hydrological Model, Water Resources Research, 55, 11166–11187, https://doi.org/10.1029/2019WR025333, 2019.

Margulis, S. A., Liu, Y., and Baldo, E.: A Joint Landsat- and MODIS-Based Reanalysis Approach for Midlatitude Montane Seasonal Snow Characterization, Front. Earth Sci., 7, 272, https://doi.org/10.3389/feart.2019.00272, 2019.

Nielsen, D. C., Unger, P. W., and Miller, P. R.: Efficient water use in dryland cropping systems in the Great Plains, Agronomy journal, 97, 364–372, https://doi.org/10.2134/agronj2005.0364, 2005.

Palomaki, R. T. and Sproles, E. A.: Assessment of L-band InSAR snow estimation techniques over a shallow, heterogeneous prairie snowpack, Remote Sensing of Environment, 296, 113744, https://doi.org/10.1016/j.rse.2023.113744, 2023.

Rosolem, R., Shuttleworth, W. J., Zreda, M., Franz, T. E., Zeng, X., and Kurc, S. A.: The Effect of Atmospheric Water Vapor on Neutron Count in the Cosmic-Ray Soil Moisture Observing System, Journal of Hydrometeorology, 14, 1659–1671, https://doi.org/10.1175/JHM-D-12-0120.1, 2013.

Royer, A., Roy, A., Jutras, S., and Langlois, A.: Review article: Performance assessment of radiation-based field sensors for monitoring the water equivalent of snow cover (SWE), The Cryosphere, 15, 5079–5098, https://doi.org/10.5194/tc-15-5079-2021, 2021.

Schattan, P., Baroni, G., Oswald, S. E., Schöber, J., Fey, C., Kormann, C., Huttenlau, M., and Achleitner, S.: Continuous monitoring of snowpack dynamics in alpine terrain by aboveground neutron sensing, Water Resour. Res., 53, 3615–3634, https://doi.org/10.1002/2016WR020234, 2017.

Schattan, P., Köhli, M., Schrön, M., Baroni, G., and Oswald, S. E.: Sensing Area-Average Snow Water Equivalent with Cosmic-Ray Neutrons: The Influence of Fractional Snow Cover, Water Resour. Res., 55, 10796–10812, https://doi.org/10.1029/2019WR025647, 2019.

https://doi.org/10.5194/egusphere-2025-31
Preprint. Discussion started: 27 January 2025

Schattan, P., Schwaizer, G., Schöber, J., and Achleitner, S.: The complementary value of cosmic-ray neutron sensing and snow covered area products for snow hydrological modelling, Remote Sensing of Environment, 239, 111603, https://doi.org/10.1016/j.rse.2019.111603, 2020.

Schrön, M., Köhli, M., Scheiffele, L., Iwema, J., Bogena, H. R., Lv, L., Martini, E., Baroni, G., Rosolem, R., Weimar, J., Mai, J., Cuntz, M., Rebmann, C., Oswald, S. E., Dietrich, P., Schmidt, U., and Zacharias, S.: Improving calibration and validation of cosmic-ray neutron sensors in the light of spatial sensitivity, Hydrol. Earth Syst. Sci., 22, https://doi.org/10.5194/hess-21-5009-2017, 2017.

Schrön, M., Köhli, M., and Zacharias, S.: Signal contribution of distant areas to cosmic-ray neutron sensors – implications for footprint and sensitivity, Hydrol. Earth Syst. Sci., 27, 723–738, https://doi.org/10.5194/hess-27-723-2023, 2023.

Serreze, M. C., Clark, M. P., Armstrong, R. L., McGinnis, D. A., and Pulwarty, R. S.: Characteristics of the western United States snowpack from snowpack telemetry (SNOTEL) data, Water Resour. Res., 35, 2145–2160, https://doi.org/10.1029/1999WR900090, 1999.

Sturm, M. and Liston, G. E.: Revisiting the Global Seasonal Snow Classification: An Updated Dataset for Earth System Applications, Journal of Hydrometeorology, https://doi.org/10.1175/JHM-D-21-0070.1, 2021.

Tsang, L., Durand, M., Derksen, C., Barros, A. P., Kang, D.-H., Lievens, H., Marshall, H.-P., Zhu, J., Johnson, J., King, J., Lemmetyinen, J., Sandells, M., Rutter, N., Siqueira, P., Nolin, A., Osmanoglu, B., Vuyovich, C., Kim, E., Taylor, D., Merkouriadi, I., Brucker, L., Navari, M., Dumont, M., Kelly, R., Kim, R. S., Liao, T.-H., Borah, F., and Xu, X.: Review article: Global monitoring of snow water equivalent using high-frequency radar remote sensing, The Cryosphere, 16, 3531–3573, https://doi.org/10.5194/tc-16-3531-2022, 2022.

Tuttle, S. E., Jacobs, J. M., Vuyovich, C. M., Olheiser, C., and Cho, E.: Intercomparison of snow water equivalent observations in the Northern Great Plains, Hydrological Processes, 32, 817–829, https://doi.org/10.1002/hyp.11459, 2018.

Woodley, M., Kim, H., Sproles, E., Eberly, J., and Tuttle, S.: Evaluating Cosmic Ray Neutron Sensor Estimates of Snow Water Equivalent in a Prairie Environment Using UAV Lidar, Water Resources Research, 60, e2024WR037164, https://doi.org/10.1029/2024WR037164, 2024.

Zeng, X., Broxton, P., and Dawson, N.: Snowpack Change From 1982 to 2016 Over Conterminous United States, Geophysical Research Letters, 45, https://doi.org/10.1029/2018GL079621, 2018.

Zreda, M., Desilets, D., Ferré, T. P. A., and Scott, R. L.: Measuring soil moisture content non-invasively at intermediate spatial scale using cosmic-ray neutrons, Geophys. Res. Lett., 35, L21402, https://doi.org/10/df2zv5, 2008.

https://doi.org/10.5194/egusphere-2025-31
Preprint. Discussion started: 27 January 2025

Zreda, M., Shuttleworth, W. J., Zeng, X., Zweck, C., Desilets, D., Franz, T., and Rosolem, R.: COSMOS: the COsmic-ray Soil Moisture Observing System, Hydrol. Earth Syst. Sci., 16, 4079–4099, https://doi.org/10.5194/hess-16-4079-2012, 2012.